

Biodegradable and flexible ι-carrageenan based RRAM with ultralow power consumption

Jing-Yao Bian(卞景垚), Ye Tao(陶冶), Zhong-Qiang Wang(王中强), Xiao-Ning Zhao(赵晓宁), Ya Lin(林亚), Hai-Yang Xu(徐海阳), and Yi-Chun Liu(刘益春)

Citation: Chin. Phys. B, 2024, 33 (**2**): 027301. DOI: 10.1088/1674-1056/ad19d4
Journal homepage: http://cpb.iphy.ac.cn; http://iopscience.iop.org/cpb

What follows is a list of articles you may be interested in

Thermal stability and data retention of resistive random access memory with HfO_x/ZnO double layers

Yun-Feng Lai(赖云锋), Fan Chen(陈凡), Ze-Cun Zeng(曾泽村), Pei-Jie Lin(林培杰), Shu-Ying Cheng(程树英), Jin-Ling Yu(俞金玲)
Chin. Phys. B, 2017, 26 (**8**): 087305. DOI: 10.1088/1674-1056/26/8/087305

Charge transport and bipolar switching mechanismin a Cu/HfO_2/Pt resistive switching cell

Tingting Tan(谭婷婷), Tingting Guo(郭婷婷), Zhihui Wu(吴志会), Zhengtang Liu(刘正堂)
Chin. Phys. B, 2016, 25 (**11**): 117306. DOI: 10.1088/1674-1056/25/11/117306

Resistive switching characteristic and uniformity of low-power HfO_x-based resistive random access memory with the BN insertion layer

Shuai Su(苏帅), Xiao-Chuan Jian(鉴肖川), Fang Wang(王芳), Ye-Mei Han(韩叶梅), Yu-Xian Tian(田雨仙), Xiao-Yang Wang(王晓旸), Hong-Zhi Zhang(张宏智), Kai-Liang Zhang(张楷亮)
Chin. Phys. B, 2016, 25 (**10**): 107302. DOI: 10.1088/1674-1056/25/10/107302

Resistive switching characteristics of Ti/ZrO_2/Pt RRAM device

Lei Xiao-Yi (雷晓艺), Liu Hong-Xia (刘红侠), Gao Hai-Xia (高海霞), Yang Ha-Ni (杨哈妮), Wang Guo-Ming (王国明), Long Shi-Bing (龙世兵), Ma Xiao-Hua (马晓华), Liu Ming (刘明)
Chin. Phys. B, 2014, 23 (**11**): 117305. DOI: 10.1088/1674-1056/23/11/117305

Effects of different dopants on switching behavior of HfO_2-based resistive random access memory

Deng Ning (邓宁), Pang Hua (庞华), Wu Wei (吴畏)
Chin. Phys. B, 2014, 23 (**10**): 107306. DOI: 10.1088/1674-1056/23/10/107306

SPECIAL TOPIC — Post-Moore era: Materials and device physics

Biodegradable and flexible ι-carrageenan based RRAM with ultralow power consumption

Jing-Yao Bian(卞景垚)[1], Ye Tao(陶冶)[1,†], Zhong-Qiang Wang(王中强)[1,2], Xiao-Ning Zhao(赵晓宁)[1], Ya Lin(林亚)[1,2], Hai-Yang Xu(徐海阳)[1,2,‡], and Yi-Chun Liu(刘益春)[1,2]

[1] *Key Laboratory of UV-Emitting Materials and Technology of Ministry of Education, Northeast Normal University, Changchun* 130024, *China*
[2] *National Demonstration Center for Experimental Physics Education, Northeast Normal University, Changchun* 130024, *China*

(Received 8 October 2023; revised manuscript received 2 November 2023; accepted manuscript online 2 January 2024)

Transient memories, which can physically disappear without leaving traceable remains over a period of normal operation, are attracting increasing attention for potential applications in the fields of data security and green electronics. Resistive random access memory (RRAM) is a promising candidate for next-generation memory. In this context, biocompatible ι-carrageenan (ι-car), extracted from natural seaweed, is introduced for the fabrication of RRAM devices (Ag/ι-car/Pt). Taking advantage of the complexation processes between the functional groups (C–O–C, C–O–H, *et al.*) and Ag metal ions, a lower migration barrier of Ag ions and a high-speed switching (22.2 ns for SET operation/26 ns for RESET operation) were achieved, resulting in an ultralow power consumption of 56 fJ. And the prepared Ag/ι-car/Pt RRAM devices also revealed the capacities of multilevel storage and flexibility. In addition, thanks to the hydrophilic groups of ι-car molecule, the RRAM devices can be rapidly dissolved in deionized (DI) water within 13 minutes, showing excellent transient characteristics. This work demonstrates that ι-car based RRAM devices have great potential for applications in secure storage applications, flexible electronics and transient electronics.

Keywords: RRAM, transient electronics, ι-carrageenan, ultralow power consumption

PACS: 73.40.Rw, 77.84.Jd, 81.07.–b **DOI:** 10.1088/1674-1056/ad19d4

1. Introduction

Various emerging electronic technologies that can provide great convenience for daily life have even thoroughly discredited our life-style in society today.[1,2] To prevent the rapid growth of global electronic waste causing severe environmental pollution, addressing electronic waste is a critical issue.[3–5] Transient electronics have the characteristics of disappearing, dissolving or degrading in a controlled way, providing new opportunities for developing the waste-free technology.[6] Transient memory is one of the most important components in transient electronics, which attracts great attention because it can offer data security by self-destruction on demand, thus avoiding sensitive information exposure.[7–9] Resistive random access memory (RRAM) is one of the most promising candidates for next-generation nonvolatile memory for simple structure, fast speed and ultra-high density storage capacity.[10,11]

Previously, various types of biodegradable materials have been employed to fabricate transient RRAM devices.[11–14] For example, Lee *et al.* reported a flexible transient RRAM device with a Mg/Ag-doped chitosan/Mg structure, which could be dissolved in deionized (DI) water.[15] Tang *et al.* demonstrated a flexible resistive switching (RS) memory of $CsPbBr_3$ thin films, which could be rapidly dissolved in DI water.[16] These works have provided effective approaches for realizing the transient characteristics of RRAM devices, promoting the development of transient memories. From these reported works we can find that most of the transient RRAM devices are electrochemical metallization (ECM) based memories.[11,12,17,18] Generally, the formation/dissolution of metallic conductive filaments (CFs) under an electric field is regarded as the physical mechanism of RS, which includes the oxidation process of Ag atoms, and the migration and reduction processes of Ag ions. However, different from traditional ECM devices, the ι-carrageenan (ι-car) molecular contains abundant functional groups, such as C–O–C and C–O–H, which can interact with metal ions. Especially, used as the insulating material of the building blocks for RRAM devices, oxygen-containing functional groups can act as the "active center" for ion conduction. The continuous interaction between these functional groups and metal ions can promote the migration of metal ions, which is one of the most desired material characteristics for developing high performance RRAM devices.[19] In addition, ι-car contains abundant hydrophilic functional groups, and water molecules can readily infiltrate into the ι-car molecular structure, facilitating the degradable process.[20]

In this work, we introduced biocompatible ι-car extracted from natural seaweed as the active layer. The tiny operating

[†]Corresponding author. E-mail: taoy506@nenu.edu.cn
[‡]Corresponding author. E-mail: hyxu@nenu.edu.cn

© 2024 Chinese Physical Society and IOP Publishing Ltd

current of 1 μA suggests that the fabricated Ag/ι-car/Pt RRAM devices consume low power. Moreover, by leveraging a high-speed pulse measurement system, we achieved an ultralow energy consumption of 56 fJ. Additionally, these ι-car-based RRAM devices also demonstrate excellent resistance switching performance, flexibility, and multilevel storage characteristics. The related mechanism was investigated via conducting atomic force microscopy (C-AFM) and temperature-dependent resistance measurements. In addition, the prepared ι-car based RRAM devices were stable in DI water at room temperature. However, it can be rapidly dissolved in water after heating, which suggests that the natural ι-car materials can be used as attractive building blocks for highly reliable transient RRAM devices.

2. Experiment

First, a SiO_2/Si substrate was ultrasonically cleaned in trichloro ethylene, acetone, ethanol, and distilled water for 12 min each to remove impurities at room temperature, then dried using N_2 gas. Secondly, 200 nm thick Pt film with 10 nm thick Ti adhesion layer was deposited by magnetron sputtering. Then, ι-car powder (commercial grade, Sigma-Aldrich, CAS number: 9062-07-1) was dissolved (1 wt/v%) in 1% acetic acid solution in distilled water with continuous stirring at 400 rpm for 24 h and then filtered through a PVDF syringe filter (0.2 μm). The Pt substrate was exposed to oxygen plasma for 5 min, then the ι-car solution (80 μL) in two drops was spin-coated on the Pt substrate at 500 rpm for 10 s and 3000 rpm for 20 s. Finally, an Ag top electrode with a diameter of 300 μm was deposited by thermal evaporation using a shadow mask.

3. Results and discussion

The ι-car was prepared through solution extraction from natural seaweed, as presented in Fig. 1(a). The ι-car extracted from seaweed was used as the RS layer. The fabricated RRAM device in this work is based on a metal–insulator–metal configuration, as shown in Fig. 1(b). To intuitively reveal the three-layer structure, the cross-sectional scanning electron microscope (SEM) image of the fabricated Ag/ι-car/Pt RRAM device is shown in Fig. 1(c). The ι-car layer with a thickness of ∼100 nm was clearly observed between the Pt bottom electrode and the Ag top electrode. The Ag-electrode-size-dependent RS measurements were also carried out (see Figs. S1 and S2, supporting information). The electrode size had no obvious influence on the RS performance, confirming the filamentary-type RS of the Ag/ι-car/Pt memory. Moreover, the fabricated ι-car film had a smooth surface of root-mean-square roughness (R_q) equal to 2.4 nm, which is demonstrated by the two-dimensional AFM image (Fig. 1(d)). These characteristics not only guarantee the material reliability of large-area ι-car thin films, but also demonstrate its application potential in flexible electronics.

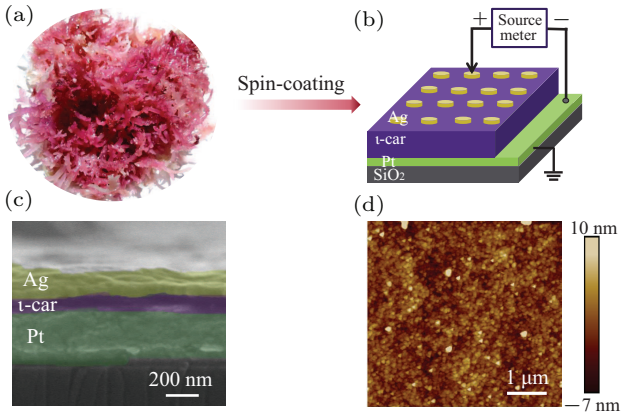


Fig. 1. (a) Seaweed image and the typical molecular structure of ι-car. (b) Structural diagram of the Ag/ι-car/Pt RRAM devices. (c) The cross-sectional SEM image of the fabricated device. (d) The AFM shows the surface morphology of the ι-car film.

First, the RS behaviors of the fabricated RRAM devices were thoroughly investigated. Figure 2(a) shows the typical current–voltage (I–V) curves of the Ag/ι-car/Pt RRAM devices. We can see that the fabricated memory cells could be written (2 V) and erased (−3 V) under the direct current (DC) voltage sweeping operation. Importantly, our Ag/ι-car/Pt RRAM devices exhibited tunable RS properties with respect to different compliance currents (CCs), i.e., 1 μA, 50 μA, 500 μA and 1 mA. The retention ability of multilevel resistance states was also demonstrated (Fig. 2(b)), and a stable retention exceeding 10^4 s under a constant read voltage of 0.1 V was observed. These five resistance states offer a unique opportunity for achieving multilevel storage. The reproducible RS measurements in Fig. 2(c) show that four distinguishable low resistance states (LRS) were obtained by varying the CCs; while the high resistance state (HRS) was basically independent of the CCs. According to some reported works,[21] the physical mechanism of the CCs-modulated multilevel storage could be associated with the size variation of CFs. From these reliable RS properties, we can deduce that the CFs of the Ag/ι-car/Pt RRAM devices can be controlled precisely, which can be related to the material characteristics of the ι-car layer, and it will be emphatically studied in the mechanism part.

In addition to excellent RS characteristics for nonvolatile storage, the device power consumption was also evaluated through the voltage sweep and pulse operation modes, as shown in Fig. 3. It is known that the power consumption of RRAM is mainly determined by the RESET current,[22,23] as shown in Fig. 3(a). Figure 3(b) shows the device power of multilevel memory states obtained at different CCs. The minimum power and RESET current of the Ag/ι-car/Pt RRAM devices were ∼ 0.3 μW and 1 μA, respectively, which are relatively low compared with those of other biodegradable mem-

ory devices.[12–14] Generally, the power consumption of RESET process is directly influenced by the last SET process. The energy consumption was precisely measured through the high-speed pulse mode. The RS time was monitored using a pulse generator (TTiTGA12104), an oscilloscope (Keysight DSOS404A), and a load resistor (1 MΩ). The pulse test electrical diagram and the results are shown in Figs. 3(c) and 3(d), respectively. The imperfect pulse waveforms and current responses could be attributed to parasitic effects in the testing circuitry.[24] The "input signal" from a waveform generator was designed as a voltage-pulse sequence, as follows: $READ1_{st}$ →SET→$READ_{1nd}$ → RESET→$READ_{2nd}$ pulse. Two READ pulses were input before and after the SET (RESET) pulse to determine whether a SET (RESET) transition occurred. The pulse amplitude/width was 2 V/50 ns for the SET pulse and 1 V/50 ns for both READ pulses. The voltage drop on the load resistor was defined as the "output signal". The switching time in the SET operation can be determined from the time delay between the "input signal" and "output signal", while the reset time can be determined from the width of the output pulse, as shown in Figs. 3(e) and 3(f). The set and reset times were approximately 22.2 ns and 26 ns, respectively. More importantly, the energy consumption of the reset process was as low as ∼ 56 fJ, which was even lower than those of the traditional oxide-based ECM devices (see Table 1).[25–29] From Table 1 we can also find that proteins-based devices have relatively high reset currents and polysaccharides-based ones demonstrate relatively low reset voltages,[13–15,17,18,30] while the RRAM devices based on ι-car material have the lowest reset current and energy consumption. All above results demonstrate that the Ag/ι-car/Pt RRAM devices exhibit the capacities of reliable high-speed switching and ultralow energy consumption.

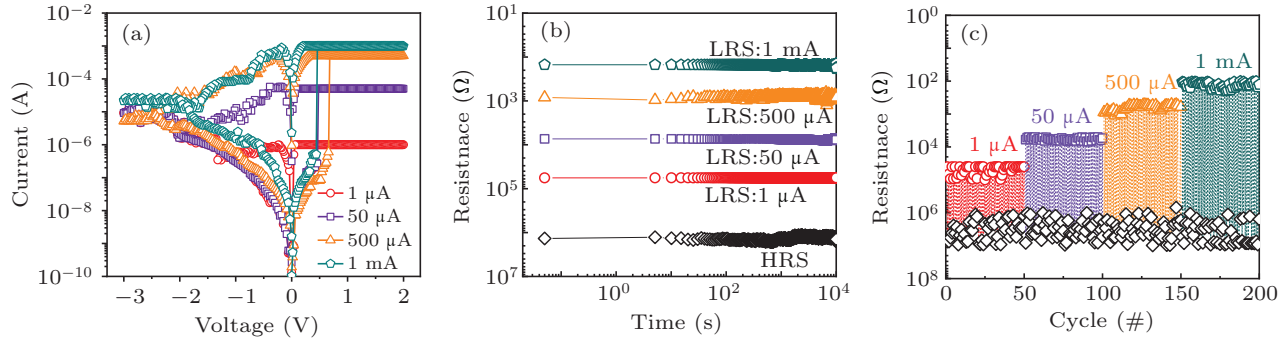


Fig. 2. (a) Typical *I*–*V* characteristics of the Ag/ι-car/Pt RRAM device under different CCs of 1 μA, 50 μA, 500 μA and 1 mA. (b) The retention characteristics of the five resistance states. (c) Statistical values of HRS and LRS under reproductive RS measurement with different CCs values.

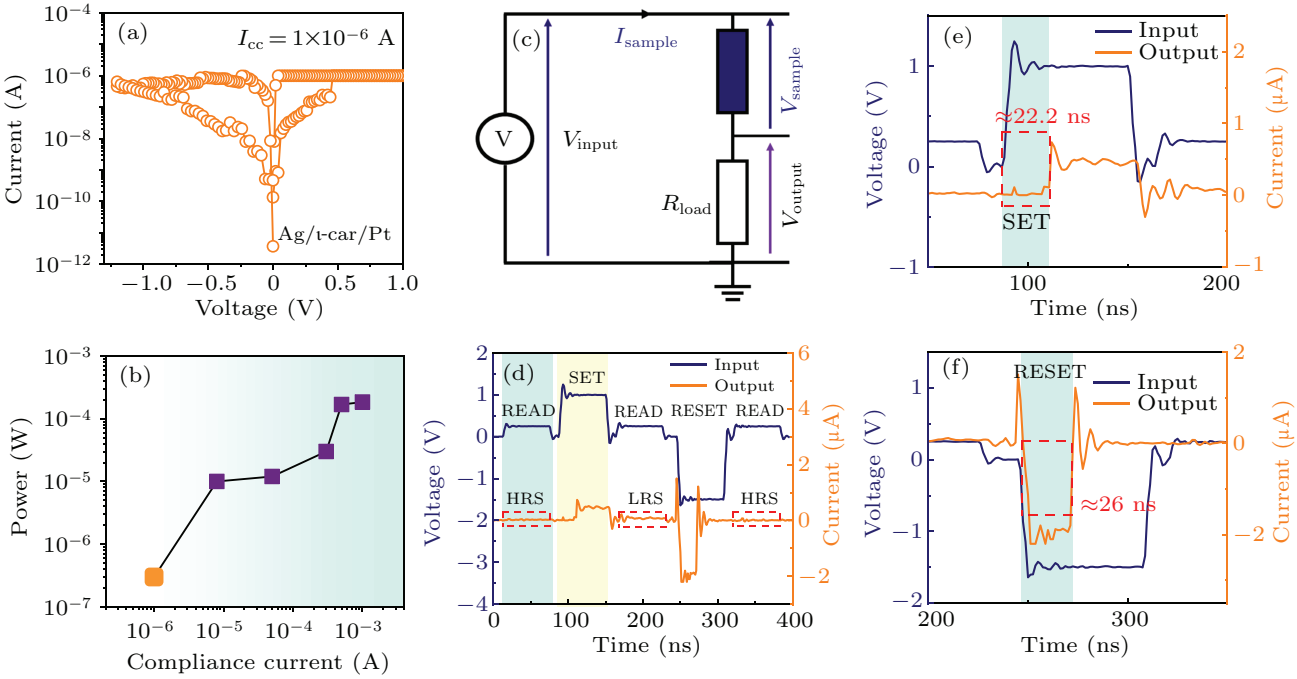


Fig. 3. (a) The *I*–*V* curves of the Ag/ι-car/Pt RRAM devices at CCs of 1 μA. (b) The variations of RESET power with different CCs for the same device. (c) Pulse test electrical schematic diagram. (d) RS-speed test of the Ag/ι-car/Pt memory devices triggered under pulse mode. Panels (e) and (f) show the set and reset time of memory cells, respectively.

Table 1. Power consumption comparisons of the present Ag/ι-car/Pt devices with those of previously reported RRAM.

Device structure	I_{reset}	$\|V_{reset}\|$	Power	T_{reset}	Energy	Ref.
Ag/keratin/FTO	1 mA	1 V	1 mW	–	–	[30]
W/egg albumen/ITO/PET	8 μA	4 V	32 μW	–	–	[13]
Ag/DNA-CTMA/ITO	0.01 A	1.2 V	12 mW	–	–	[17]
Mg/Ag-doped chitosan/Mg	0.01 A	1 V	10 mW	–	–	[15]
Ag/silk fibroin/Au	0.1 μA	4 V	0.4 μW	–	–	[18]
ITO/2D/3D perovskite/Au	3.5 μA	1 V	3.5 μW	1 μs	35 pJ	[25]
W/silk fibroin/Mg/SiO_2	1 mA	2.2 V	2.2 mW	–	–	[14]
Pt/Cu-DNA/FTO	0.01 A	2.5 V	25 mW	–	–	[31]
Al/glucose/Si	1 mA	2 V	2 mW	–	–	[32]
Ag/GeSe/TiN	0.1 mA	1 V	0.1 mW	–	300 pJ–12 nJ	[33]
Cu/AlO_x/a-CO_x/TiN_xO_y/TiN	0.22 mA	0.48 V	0.1 mW	–	6.7 pJ–13.3 pJ	[26]
Au/$CH_3NH_3PbI_3$/FTO	1 mA	0.5 V	0.5 mW	156 ns	468 pJ	[27]
$LiCoO_2$/SiO_x/TiO_2	0.6 mA	5 V	3 mW	–	–	[28]
Ag/leaves/Ti	4 mA	0.75 V	3 mW	–	–	[12]
Al/Cu/Ti/MoS_2/Pt	0.025 mA	0.15 V	3.8 μW	–	0.7 pJ	[29]
Ag/ι-car/Pt/SiO_2/Si	1 μA	0.3 V	0.3 μW	26 ns	56 fJ	this work

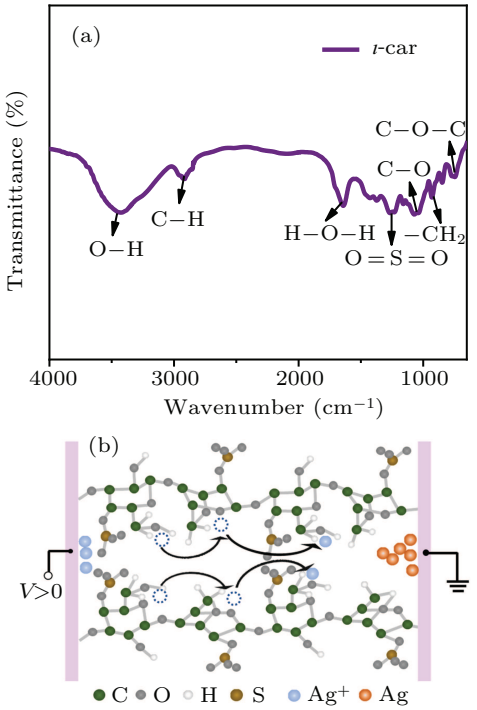


Fig. 4. (a) FTIR spectrum of the ι-car thin film. (b) Schematic diagram of Ag migration mechanism.

The functional groups of the ι-car were identified using Fourier-transform infrared spectrum (FTIR), as shown in Fig. 4(a), which was obtained using transmittance mode in the range 650–4000 cm^{-1}. The spectrum revealed the presence of multifarious functional groups, such as C–O, C–O–C, C–H, and O=S=O.[34] These oxygen-containing functional groups play an important role in the process of RS. As shown in Fig. 4(b), when a positive voltage is applied to the Ag electrode, oxidized Ag metal ions can migrate by interacting with these functional groups (C–O–C, C–O–H, *et al.*),[20] thus the CFs will preferentially grow along the locations rich in functional groups.[35] And when a negative voltage is applied to the Ag electrode, Joule-heating-assisted electrochemical dissolution process occurs, thus CFs break in the weakest region. The formation and rupture of CFs contribute to the repeatable RS.

The activation energy could be roughly equal to the sum of the migration barriers,[36,37] which would change due to mechanical stresses caused by thermal expansion. To evaluate the activation energy coefficient and the effect of temperature on switching time, we performed a temperature change test. As shown in Fig. 5(a), the V_{SET} was primarily determined by the barrier energy for Ag-migration, which could be estimated by measuring the SET switching time as a function of temperature.[38,39] As shown in Fig. 5(b), the switching time was sensitive to temperature, which decreased exponentially and can be expressed based on the Arrhenius relation as follows:[40,41]

$$t \propto \exp(-E_a/k_B T), \tag{1}$$

where E_a, k_B and T are the barrier energy, Boltzmann constant, and temperature, respectively. As shown in Fig. 5(c), the barrier energy was calculated from the slope of the Arrhenius plots, which yielded 0.2 eV for the devices with abundant hydroxyl functional groups. The lower migration barrier of Ag ions in RS insulating layer could have contributed to the V_{SET} reduction and low power consumption.

On the basis of the calculated results of activation energy, we will discuss the possible physical mechanism for low power operation of Ag/ι-car/Pt memory cells as follows. Lee *et al.* demonstrated the ultralow power consumption biomemristors of Ag/Ag-doped CM:κ-car/Pt RRAM devices by introducing carboxymethyl (CM) groups.[42] Oxygen atoms containing lone pair electrons can serve as "active centers" for ions conduction, and water molecules coordinate with the lone pair electrons to the vacant orbital (primarily hybrid orbital) of the Ag ions, which form electrovalence or covalent coordination bonds with Ag ions,[19] moreover, the functional groups

(C–O–C and C–O–H) can form cross-linking networks with other components in the polymer electrolyte and enable complexation with metal ions.[20,42,43] Therefore, it is more easier for Ag metal ions to migrate in the polymers containing functional groups, which is the root reason of lower power consumption for our Ag/ι-car/Pt memory cells.

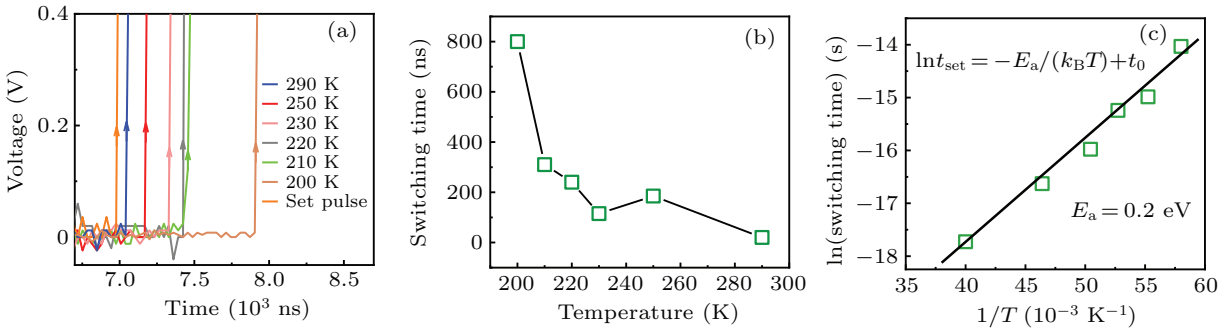


Fig. 5. (a) SET switching response of Ag/ι-car/Pt memory cells under different temperatures. (b) Temperature dependence of SET switching time for the memory cells, as well as (c) Arrhenius plots for determining migration barrier energy (E_a).

To further investigate the conductive path during the RS process, C-AFM was also performed to analyze both the HRS and LRS. The conductive cantilever was scanned over an area of 1 μm×1 μm and the read voltage was set to 100 mV. As shown in Fig. 6(a), the current value at HRS was very low and no remarkable localized current paths were observed. In contrast, when the RRAM device was switched to the LRS (CC∼ 1 μA), two tiny localized current paths emerged, as shown in Fig. 6(b), indicating the formation of nanometer-scale conducting channels. To demonstrate the RS mechanism of the Ag/ι-car/Pt RRAM devices, the temperature-dependent resistance measurement of LRS is shown in Fig. 6(c), the resistance decreased linearly with the temperature, confirming the formation of CFs after the set switching process. After linearly fitting the data, it is found that the temperature coefficient (α) is approximately equal to 4.7×10^{-3} K^{-1}, close to that of pure silver (3.8×10^{-3} K^{-1}).[11,44]

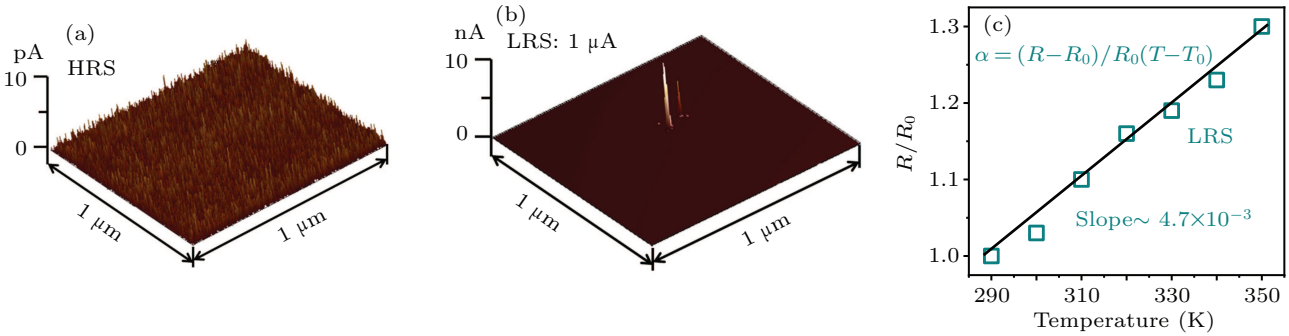


Fig. 6. The local conductivity distribution of the Ag/ι-car/Pt memory in (a) HRS, (b) LRS at CCs of 1 μA. (c) Temperature-dependent resistance measurement of LRS.

Additionally, to evaluate the mechanical flexibility of the device, we performed bending tests. As shown in Fig. 7(a), we fabricated RRAM devices on a polyethylene terephthalate (PET) substrate coated with ITO film (Ag/ι-car/ITO/PET). The ι-car memristor cells with the ITO electrode showed similar RS characteristics (Fig. S3). As shown in Fig. 7(b), the HRS/LRS and V_{set}/V_{reset} parameters were minimally affected after bending with different radii, i.e., 10 mm, 15 mm, 20 mm and 25 mm. In addition, the flexible RRAM devices also exhibited good mechanical stability without significant degradation during repeated bending over 10^3 cycles at a bending radius of 20 mm (one bending cycle means that the device is returned to the flat state after bending with a fixed curvature). The maintenance of the performance is probably due to the short vertical channel of nanometer scale and the ductility of the materials, which suggests their reliable RRAM characteristics and excellent mechanical properties.

The introduction of ι-car containing abundant hydrophilic functional groups into RRAM devices enables the transient behavior achievement. The fabricated Ag/ι-car/ITO/PET memory devices were straightway immersed into DI water with a temperature of approximately 26 °C. Whereafter, the devices were transferred into another culture dish full of DI water with temperature of 80 °C. For comparison, we chose to heat the device uniformly with microwaves to 80 °C, observed for 10 min, and found that the thin film of the device still existed (Fig. S4). Figures 8(a) and 8(b) show the sequential images of the dissolution process of the Ag/ι-car/ITO/PET RRAM devices. We can find that the electrode

destroyed gradually and the ι-car film disappeared completely. The clean ITO/PET substrate was only left in the culture dish after 13 min. This indicates that the ι-car based RRAM devices can effectively avoid the recycling costs of discarded electronic waste, thereby facilitating the development of environmentally friendly electronics and data protection.

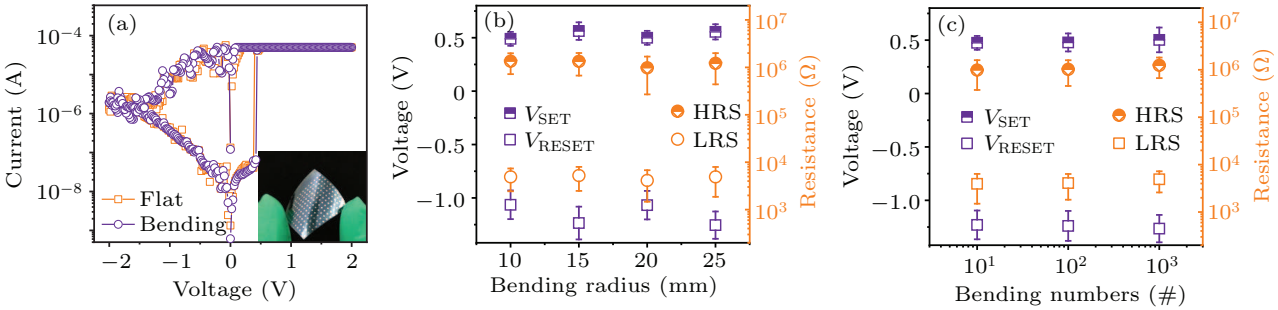


Fig. 7. (a) The *I*–*V* curves of memory devices at flat and high bending deformation states. Inset: The photograph of the device under bending state. (b) Flexibility test results of Ag/ι-car/ITO/PET RRAM devices for various bending radii under tensile strain. (c) Mechanical bending endurance of Ag/ι-car/ITO/PET memory devices at bending radius of 20 mm.

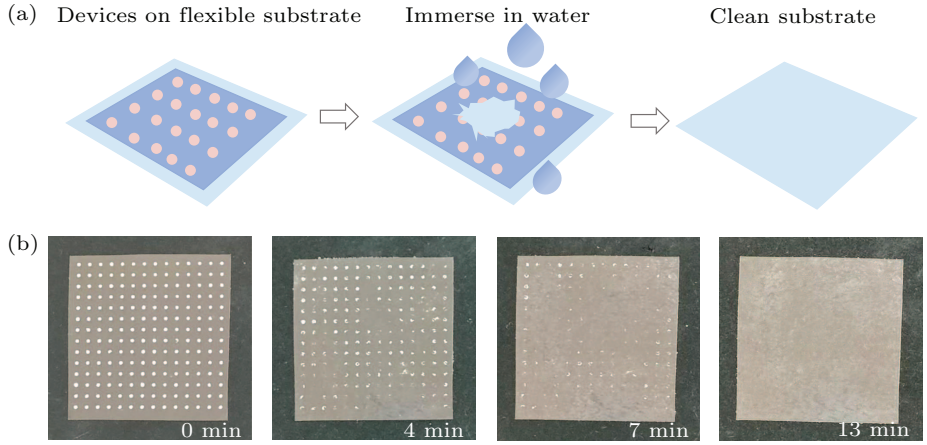


Fig. 8. (a) Schematic illustrations (a) and the photographs (b) demonstrating disappearing process of the Ag/ι-car/ITO/PET RRAM devices in DI water.

4. Conclusion and perspectives

In summary, biodegradable ι-car based RRAM devices with a cell structure of Ag/ι-car/Pt were fabricated. Remarkable RS characteristics, such as fast switching speed (∼ 26 ns), multilevel storage behaviors, and excellent bending performance (∼ 10^3 cycles) have been achieved for nonvolatile flexible memory applications. Due to the complexation between Ag metal ions and the oxygen-containing functional groups, an ultralow power consumption of ∼ 56 fJ was achieved, which is much lower than that of most reported transient RRAM devices. In addition, the devices can completely disappear while immersed in DI water after 13 min, demonstrating the excellent transient characteristics. The demonstrated Ag/ι-car/Pt transient RRAM devices offer great potential for flexible electronics and green electronics.

The transient electronic devices can be used to manufacture transient environmental monitoring devices, which can self-destroy after a certain period of time, reducing their impact on the environment. This is very useful for long-term monitoring and data collection in the environment. In future, transient electronic devices can also be used for security and privacy protection.

Acknowledgements

This work is supported financially by the National Key Research and Development Program of China (Grant No. 2023YFB4402301), the National Science Fund for Distinguished Young Scholars (Grant No. 52025022), the National Natural Science Foundation of China (Grant Nos. U19A2091, 62004016, 51732003, 52072065, 11974072, 52372137, and 52272140), the "111" Project (Grant No. B13013), the Fundamental Research Funds for the Central Universities (Grant Nos. 2412022QD036 and 2412023YQ004) and the funding from Jilin Province (Grant Nos. 20210201062GX, 20220502002GH, 20230402072GH, 20230101017JC, and 20210509045RQ).

References

[1] Kenry, Yeo J C and Lim C T 2016 *Microsyst. Nanoeng.* **2** 16043
[2] Bhatia M and Sood S K 2016 *J. Med. Syst.* **40** 190
[3] Shim J S, Rogers J A and Kang S K 2021 *Mater. Sci. Eng. R Rep.* **145** 100624
[4] Kiddee P, Naidu R and Wong M H 2013 *Waste Manage* **33** 1237

[5] Gollakota A R K, Gautam S and Shu C M 2020 *J. Environ. Manage* **261** 110234
[6] Feng S X, Cao S T, Tian Z S, Zhu H Y and Kong D S 2019 *ACS Appl. Mater. Interfaces* **11** 45844
[7] Hernandez H L, Kang S K, Lee O P, Hwang S W, Kaitz J A, Inci B, Park C W, Chung S J, Sottos N R, Moore J S, Rogers J A and White S R 2014 *Adv. Mater.* **26** 7637
[8] Park C W, Kang S K, Hernandez H L, Kaitz J A, Wie D S, Shin J, Lee O P, Sottos N R, Moore J S, Rogers J A and White S R 2015 *Adv. Mater.* **27** 3783
[9] Lee C H, Kang S K, Salvatore G A, Ma Y J, Kim B H, Jiang Y, Kim J S, Yan L Q, Wie D S, Banks A, Oh S J, Feng X, Huang Y G, Troester G and Rogers J A 2015 *Adv. Funct. Mater.* **25** 5100
[10] Park S P, Tak Y J, Kim H J, Lee J H, Yoo H and Kim H J 2018 *Adv. Mater.* **30** 1800722
[11] Xu J Q, Zhao X N, Wang Z Q, Xu H Y, Hu J L, Ma J G and Liu Y C 2018 *Small* **15** 1803970
[12] Sun B, Zhu S H, Mao S S, Zheng P P, Xia Y D, Yang F, Lei M and Zhao Y 2018 *J. Colloid Interface Sci.* **513** 774
[13] Yan X B, Li X Y, Zhou Z Y, Zhao J H, Wang H, Wang J J, Zhang L, Ren D L, Zhang X, Chen J S, Lu C, Zhou P and Liu Q 2019 *ACS Appl. Mater. Interfaces* **11** 18654
[14] Ji X L, Song L, Zhong S, Jiang Y, Lim K G, Wang C and Zhao R 2018 *J. Phys. Chem. C* **122** 16909
[15] Hosseini N R and Lee J S 2015 *Adv. Funct. Mater.* **25** 5586
[16] Lin Q Q, Hu W, Zang Z G, Zhou M, Du J, Wang M, Han S and Tang X S 2018 *Adv. Electron. Mater.* **4** 1700596
[17] Jeng H Y, Yang T C, Li Y, Grote J G, Chen H L and Hung Y C 2018 *Org. Electron.* **54** 216
[18] Kook G, Jeong S, Kim M K, Lee S, Choi N and Lee H J 2020 *Adv. Mater. Technol.* **5** 1900991
[19] Su'ait M S, Ahmad A, Hamzah H and Rahman M Y A 2009 *J. Phys. D: Appl. Phys.* **42** 055410
[20] Kim M K and Lee J S 2018 *ACS Nano* **12** 1680
[21] Wang Z Q, Li X H, Xu H Y, Wang W, Yu H, Zhang X T, Liu Y X and Liu Y C 2010 *J. Phys. D: Appl. Phys.* **43** 385105
[22] Shi K X, Xu H Y, Wang Z Q, Zhao X N, Liu W Z, Ma J G and Liu Y C 2017 *Appl. Phys. Lett.* **111** 223505
[23] Zhao X N, Wang Z Q, Li W T, Sun S W, Xu H Y, Zhou P, Xu J Q, Lin Y and Liu Y C 2020 *Adv. Funct. Mater.* **30** 1910151
[24] Zhang T, Yin M H, Xu C M, Lu X Y, Sun X H, Yang Y C and Huang R 2017 *Nanotechnology* **28** 455202
[25] Sun K X, Wang Q R, Zhou L, Wang J J, Chang J J, Guo R, Tay B K and Yan X B 2023 *Sci. China Mater.* **66** 2013
[26] Ginnaram S, Qiu J T and Maikap S 2020 *ACS Omega* **5** 7032
[27] Zhang X H, Zhao X N, Shan X Y, Tian Q L, Wang Z Q, Lin Y, Xu H Y and Liu Y C 2021 *ACS Appl. Mater. Interfaces* **13** 28555
[28] Wang J R, Zhuge X and Zhuge F 2021 *Sci. Technol. Adv. Mater.* **22** 326
[29] Dutta M, Senapati A, Ginnaram S and Maikap S 2020 *Vacuum* **176** 109326
[30] Lin Q Q, Hao S L, Hu W, Wang M, Zang Z G, Zhu L N, Du J and Tang X S 2019 *J. Mater. Chem. C* **7** 3315
[31] Abbas Y, Dugasani S R, Raza M T, Jeon Y R, Park S H and Choi C 2019 *Nanotechnology* **30** 335203
[32] Park S P, Tak Y J, Kim H J, Lee J H, Yoo H and Kim H J 2018 *Adv. Mater.* **30** 1800722
[33] Sun Y, Xu H, Liu S, Song B, Liu H J, Liu Q and Li Q J 2018 *IEEE Electron. Device Lett.* **39** 492
[34] Chitra R, Sathya P, Selvasekarapandian S and Meyvel S 2020 *Mater. Res. Express* **7** 015309
[35] Kang Y H, Lee T I, Moon K J, Moon J W, Hong K, Cho J H, Lee W and Myoung J M 2013 *Mater. Chem. Phys.* **138** 623
[36] He K N, Kong X S and Liu C S 2020 *Comput. Mater. Sci.* **184** 109948
[37] Sundell P G, Björketun M E and Wahnström G 2007 *Phys. Rev. B* **76** 094301
[38] Seung H M, Kwon K C, Lee G S and Park J G 2014 *Nanotechnology* **25** 435204
[39] Huang Y H, Chen H A, Wu H H and Hsieh T E 2015 *J. Appl. Phys.* **117** 014505
[40] Ling H F, Tan K M, Fang Q Y, Xu X S, Chen H, Li W W, Liu Y F, Wang L Y, Yi M D, Huang R, Qian Y, Xie L H and Huang W 2017 *Adv. Electron. Mater.* **3** 1600416
[41] Zhao X N, Wang Z Q, Xie Y, Xu H Y, Zhu J X, Zhang X T, Liu W Z, Yang G C, Ma J G and Liu Y C 2018 *Small* **14** 1801325
[42] Kim M K and Lee J S 2018 *ACS Appl. Mater. Interfaces* **10** 10280
[43] Yang Y, Hu H, Zhou C H, Xu S, Sebo B and Zhao X Z 2011 *J. Power Sources* **196** 2410
[44] Ji S L, He W W, Wang K, Ran Y X and Ye C H 2014 *Small* **10** 4951